Monthly Notices
of the
ROYAL ASTRONOMICAL SOCIETY

Mon. Not. R. Astron. Soc. **416,** 1822–1835 (2011) doi:10.1111/j.1365-2966.2011.19162.x

Secondary infall model and dark matter scaling relations in intermediate-redshift early-type galaxies

V. F. Cardone,[1,2⋆] A. Del Popolo,[3] C. Tortora[4] and N. R. Napolitano[5]

[1] *I.N.A.F. – Osservatorio Astronomico di Roma, via Frascati 33, 00040 Monte Porzio Catone, Roma, Italy*
[2] *Dipartimento di Scienze Fisiche, Università degli Studi di Napoli 'Federico II', Complesso Universitario di Monte Sant'Angelo, Edificio N, via Cinthia, 80126 Napoli, Italy*
[3] *Dipartimento di Fisica e Astronomia, Università di Catania, Viale Andrea Doria 6, 95125 Catania, Italy*
[4] *Universität Zürich, Institut für Theoretische Physik, Winterthurerstrasse 190, CH-8057 Zürich, Switzerland*
[5] *INAF – Osservatorio Astronomico di Capodimonte, Salita Moiariello 16, I-80131 Napoli, Italy*

Accepted 2011 May 30. Received 2011 April 29; in original form 2010 December 13

ABSTRACT

Scaling relations among dark matter (DM) and stellar quantities are a valuable tool to constrain formation scenarios and the evolution of galactic structures. However, most of the DM properties are actually not directly measured, but derived through model-dependent mass-mapping procedures. It is therefore crucial to adopt theoretically and observationally well founded models. We use here an updated version of the secondary infall model (SIM) to predict the halo density profile, taking into account the effects of angular momentum, dissipative friction and baryons collapse. The resulting family of halo profiles depends only on one parameter, the virial mass, and nicely fits the projected mass and aperture velocity dispersion of a sample of intermediate redshift lens galaxies. We derive DM-related quantities (namely the column density and the Newtonian acceleration) and investigate their correlations with stellar mass, luminosity, effective radius and virial mass.

Key words: galaxies: elliptical and lenticulars, cD – galaxies: formation – galaxies: kinematics and dynamics – dark matter.

1 INTRODUCTION

According to the concordance ΛCDM model (Carroll, Press & Turner 1992), dark energy (in the form of a cosmological constant or a varying scalar field) and dark matter (hereafter, DM) are the dominant actors on the cosmological scene (Komatsu et al. 2009; Lampteil et al. 2010; Percival et al. 2010). In particular DM represents most of the total mass on galactic and cluster scales and drives the formation and evolution of cosmic structures. Roughly speaking, DM haloes form when the expanding matter within (and surrounding) an overdense region experiences deceleration because of the gravitational force, decouples from the Hubble flow, collapses and eventually virializes. Models including all these processes have been realized using different approaches.

N-body simulations have been the primary instrument to fully implement the non-linearities of the formation process which are realized in the dark halo growth. Even though they cannot make a full understanding of the physics of galaxy formation possible, collisionless simulations have been successful in reproducing a wide range of galaxy properties, e.g. the spherically averaged halo density profile, $\rho_{\rm DM}(r)$, which has been found to be well described by a double power-law relation with $\rho_{\rm DM} \propto r^{-3}$ in the outer regions and $\rho_{\rm DM} \propto r^{-\alpha}$ at their centres with the exact value of α remaining a matter of controversy. In the popular NFW model (Navarro, Frenk & White 1997) they find $\alpha = 1$ independently on halo mass, while either a steeper $\alpha = 1.5$ (Moore et al. 1998; Ghigna et al. 2000; Fukushige & Makino 2001; Mamon & Lokas 2005) or even shallower values (e.g. Power et al. 2003; Fukushige, Kawai & Makino 2004; Navarro et al. 2004) have been claimed elsewhere. It is also possible that α is not universal at all, but rather dependent on halo mass, merger history and substructures (Jing & Suto 2000; Klypin et al. 2001).

On the contrary, semi-analytical models are more flexible, offering the possibility to include a vast variety of physical ingredients. In particular, Gunn & Gott (1972), Gott (1975) and Gunn (1977) introduced the secondary infall model (SIM) to describe the collapse and virialization of haloes that are spherically symmetric, have suffered no major mergers and have undergone quiescent accretion. After these first analyses, other works have relaxed the assumption of purely radial self-similar collapse by including non-radial motions arising from secondary perturbations and taking care of both angular momentum and stars to lead shallower or steeper density profiles depending on the halo mass (see, e.g., Del Popolo 2010 and references therein).

⋆E-mail: winnyenodrac@gmail.com

Numerical and semi-analytic models generally lead to different predictions which need a detailed observational scrutiny. Furthermore, the adoption of the proper density model is the basic ingredient to derive the global DM properties which are critical parameters in the galaxy formation scenario: e.g. the virial mass which is considered the driver of the heating process that might affect the star formation history (Dekel & Birnboim 2006; Cattaneo et al. 2008) and the overall star formation efficiency (Conroy & Wechsler 2009).

From this point of view, scaling relations among DM and stellar quantities may provide an important test to constrain both the formation scenarios and the DM properties. Early-type galaxies (ETGs) are the ideal tools for these aims. First of all they are found to lie on the so-called Fundamental Plane (FP) which tightly relates the central velocity dispersion, effective radius and surface brightness. In particular, the well-known deviation (or 'tilt') of the FP with respect to the expectation of the virial theorem is still to be fully understood. The different explanations proposed rely in turn on non-homology, variations in the stellar M/L ratio with luminosity and a varying DM content (see, e.g. Busarello et al. 1997; D'Onofrio et al. 2006; Tortora et al. 2009, T+09 hereafter). Each of these solutions may tell a different story about the interplay between the DM and the stellar component, thus, it is clear how the constraints on scaling relations can help to shed light on the formation and evolutionary processes.

Recently, there have been growing evidences that the DM mass fraction in the ETGs' central regions is an increasing function of stellar mass (or luminosity) hence supporting the idea that DM might be the main driver of the FP tilt (Cappellari et al. 2006; Bolton 2007; Cardone et al. 2009; Hyde & Bernardi 2009; T+09; Auger et al. 2010). On the other hand, the mean 3D DM central density has been found to decrease with mass and luminosity (Thomas et al. 2009, T+09, Tortora et al. 2010), while there are contradictory results on the universality of the column density $\mathcal{S}_{\rm DM} = M_{\rm DM,proj}/\pi R^2$ (where $M_{\rm DM,proj}$ is the projected DM mass within the radius R) with some results arguing for its constancy over 12 orders of magnitude in luminosity (Donato et al. 2009; Gentile et al. 2009) and other works finding a correlation with halo mass (Boyarsky et al. 2009). Part of this controversy may probably be ascribed to the different assumptions on the halo model and stellar initial mass function (IMF) or the adopted scale radius, as recently argued by some of us (Cardone & Tortora 2010, hereafter CT10). On the other hand, it is also possible that $\mathcal{S}_{\rm DM}$ changes with the morphological type as suggested by the recent results in Napolitano, Romanowsky & Tortora (2010), where the central projected density in ETGs is found to be, on an average, systematically higher than the same quantity for spiral and dwarf galaxies (see also Boyarsky et al. 2009, hereafter B09).

In order to further investigate this issue, we present here the analysis of the above scaling relations based on the SIM density profile obtained in Del Popolo (2010) adding to the usual recipe of the gravitational collapse, the effects of ordered and random angular momentum, dynamical friction and adiabatic contraction (AC) due to the baryonic collapse.

We use the Einstein radius and velocity dispersion data from a sample of intermediate redshift ($\langle z\rangle \simeq 0.2$) lens galaxies from the Sloan Lens ACS (SLACS) survey (Auger et al. 2009, A+09, hereafter) to constrain the model parameters and derive different scaling relations. A general overview of the model is given in Section 2, while in Section 3 we introduce the lens sample and describe the fitting procedure. Our main results are shown in Section 4 and discussed in the concluding section, Section 5.

2 THE HALO MODEL

The density profile of DM haloes is obtained here by using the analytical method described in Del Popolo (2009, hereafter DP09) to which we refer the interested reader for more details. Here we give a brief description of the model properties that are of main interest for our aims.

The halo profiles are derived by assuming the secondary infall model (Gunn & Gott 1972) where a bound mass shell of the initial comoving radius x_i expands up to a maximum radius (or turnaround radius) $x_{\rm ta}$. As successive shells expand, they an acquire angular momentum and then contract on orbits determined by the angular momentum itself, while dissipative processes and eventual violent relaxation intervene to virialize the system converting kinetic energy into random motions. The final density profile may then be computed as

$$\rho(x) = \frac{\rho_{\rm ta}(x_{\rm ta})}{(x/x_{\rm ta})^3}\left[1 + \frac{{\rm d}\ln(x/x_{\rm ta})}{{\rm d}\ln x_{\rm ta}}\right] \quad (1)$$

with $\rho_{\rm ta}(x_{\rm ta})$ the density at turnaround and $x/x_{\rm ta}$ referred to as the collapse factor (see equation A18 in DP09). To describe the protohaloes density profile, DP09 considered the profile of a peak in the density field generated according to the Baarden et al. (1986) power spectrum and then took into account angular momentum, dynamical friction and the presence of baryons following the steps described below.

First, the angular momentum is decomposed in an ordered component, related to the tidal torques experienced by protohaloes, and a random component connected with random velocities (Ryden & Gunn 1987). The ordered term is computed following Ryden (1988), while the random part is assigned to protostructures according to Avila-Reese, Firmani & Hernandez (1998). A term related to the dynamical friction force has been explicitly introduced in the equations of motion and evaluated Kandrup (1980) dividing the gravitational force into an average and a random component generated by the clumps in the hierarchical universe. Finally, some adiabatic contraction of the halo, due to the baryonic collapse, has been taken into account through the formalism of Klypin, Zhao & Somerville (2002) and Gnedin et al. (2004), also including the exchange of angular momentum among baryons and dark matter.

The final product of this halo formation method gives the DM density profile as a function of the radius r and the total halo mass $M_{\rm vir}$. The latter is the only parameter needed in order to specify the halo density, being the halo inner slope α a function of the virial mass as well. As discussed in DP10, the dependence of α on $M_{\rm vir}$ breaks the universality of the halo profiles and favour Burkert (1995) models at dwarf scales, and models steeper than NFW at normal galaxy scales.

For the analysis we want to propose in the following, it is more convenient to handle some analytical halo density profile, thus we decided to approximate the numerical DP10 models with a generalized NFW density profile (Jing & Suto 2000), which allows us to accommodate the varying inner slope α as[1]

$$\rho_{\rm DM}(r,z) = \Delta_{\rm vir}\rho_{\rm crit}(z)\left(\frac{r}{R_{\rm vir}}\right)^{-\gamma}\left(1+\frac{c_{\rm vir}r}{R_{\rm vir}}\right)^{-(3-\gamma)}, \quad (2)$$

[1] The adoption of an analytical approximation to the numerical output of the model will make the adoption of the DP09 results easier to handle in the mass mapping proposed below.

where $\rho_{\rm crit}(z) = 3H^2(z)/8\pi G$ is the critical density[2] of the Universe at redshift z and $c_{\rm vir} = R_{\rm vir}/R_{\rm s}$ is the halo concentration (with $R_{\rm s}$ and $R_{\rm vir}$ the radius where the logarithmic density slope equals -2 and the virial radius, respectively). Differently from the original SIM we want to approximate (which is fully assigned by the halo mass only), the generalized NFW profile is formally a function of two parameters, namely ($c_{\rm vir}$, $M_{\rm vir}$). Thus, in equation (2), the dependence on $c_{\rm vir}$ is fictitious and we can fit the same halo profile with different $c_{\rm vir}$ values by changing the corresponding $\Delta_{\rm vir}$. Due to this liberty in the $c_{\rm vir}$ choice, we therefore arbitrarily scale $c_{\rm vir}$ with the total mass $M_{\rm vir}$ using the popular relation (Bullock et al. 2001)

$$c_{\rm vir} = 12.81 \left(\frac{M_{\rm vir}}{10^{12}\,{\rm M}_\odot}\right)^{-0.13}, \tag{3}$$

and then fit for $\Delta_{\rm vir}$ as a function of $c_{\rm vir}$ obtaining

$$\Delta_{\rm vir} \simeq \frac{6.626\times10^{-3}}{c_{\rm vir}^{0.1}}\left\{c_{\rm vir}^3\left[\ln(1+c_{\rm vir}) - \frac{c_{\rm vir}}{1+c_{\rm vir}}\right]\right\}^{2.1}. \tag{4}$$

With the chosen set-up, the analytic expression of the inner logarithmic slope γ as a function of the mass ($M_{12} = M_{\rm vir}/10^{12}\,{\rm M}_\odot$) turns out to be written as

$$\gamma \simeq 0.62 + \frac{1.166M_{12}^{1/3} - 1}{1.166M_{12}^{1/3} + 1}. \tag{5}$$

We have checked that this analytical model fits extremely well the numerical density profile over the mass range $10^{10} \leq {\rm M/M}_\odot \leq 10^{14}$ and is fully described by the virial mass as a single parameter, as prescribed by the SIM numerical results. Moreover, it is worth stressing that the use of the above $c_{\rm vir}$–$M_{\rm vir}$ relation is just a convenient choice to simplify the search for an analytical approximation which does not affect the final accuracy of the numerical SIM profile fitting.[3]

As a final remark, we warn the reader that the above fitting formulae for $\Delta_{\rm vir}$ versus $c_{\rm vir}$ and γ versus $M_{\rm vir}$ have been obtained by considering haloes at $z = 0$ (since there is a larger statistics and better resolution), while we will adopt it also at the intermediate redshifts of the lenses we will consider later. As can be seen from fig. 2 in Del Popolo (in preparation), the evolution of γ with z is actually quite small from $z = 0$ to 1 over the mass range of interest here so that we prefer to rely on these well-checked approximations rather than trying to fit less numerically accurate higher z profiles.

3 TESTING THE SIM MODEL

There are two main characteristics of the SIM halo model obtained above that make it particularly interesting: (i) it is theoretically well founded and intuitively incorporates most of the dark and baryonic collapse physics, and (ii) it ends up with a halo family which depends on a single parameter (the virial mass) and can be written analytically as a generalized NFW (once specified the dependence of the halo normalization on the NFW parameter $c_{\rm vir}$).

As a first observational test for this halo model, we start with a sample of ETGs for which we can use a multitechnique approach as in CT10. The sample includes 59 ETGs from the lenses catalogue collected by the SLACS survey (Auger et al. 2009, hereafter A+09) for which the velocity dispersion $\sigma_{\rm ap}$ (within a circular aperture of radius $R_{\rm ap} = 1.5$ arcsec) and the Einstein radius $R_{\rm E}$, and hence the projected mass within it, $M_{\rm E} = M_{\rm proj}(R_{\rm E})$, are measured. Following A+09, we will model the light distribution with a de Vaucouleurs (1948) profile with the effective radius $R_{\rm e}$ and total luminosity L_V set to the values inferred from the V-band photometry. Finally, we use the estimate of the total stellar mass, $M_\star$, from the SLACS team (A+09, table 4) where a Salpeter (1955) IMF is assumed.

The median values of $R_{\rm ap}/R_{\rm e}$ and $R_{\rm E}/R_{\rm e}$ (respectively 0.62 and 0.51) indicate that the data probe the galaxy inner regions where we need to carefully account for the stellar contribution to the model estimates of $\sigma_{\rm ap}$ and $M_{\rm E}$. To this end, we adopt the PS model (Prugniel & Simien 1997) as its projection closely mimics the Sérsic (1968) surface brightness profile and provides an analytical form of the physical quantities of interest.

With the projected profile being a Sersic model, the lensing properties of the PS model are also analytically computed (Cardone 2004; Eliasdottir & Møller 2007). In particular, the projected mass within $\xi = R/R_{\rm e}$ is

$$M_\star^{\rm proj}(\xi) = M_\star\left[1 - \frac{\Gamma(b_n\xi^{1/n})}{\Gamma(2n)}\right] \tag{6}$$

where $M_\star$ is total stellar mass, $\Gamma(x, y)$ and $\Gamma(x)$ are incomplete and complete Γ functions, and we set $n = 4$ to mimic the deprojected de Vaucouleurs (1948) profile used by the SLACS team to fit the surface brightness of their galaxies.

The stellar and DM mass models are finally used as input for the computation of the luminosity-weighted velocity dispersion profile. As a first step, the line-of-sight velocity dispersion is given by (Mamon & Lokas 2005)

$$I(R)\sigma_{\rm los}^2(R) = \frac{GM_{\rm e}\rho_\star^{\rm e}}{\Upsilon_\star}\int_\xi^\infty \frac{K(\eta/\xi)\tilde\rho_\star(\eta)\tilde M_{\rm tot}(\eta)}{\eta}{\rm d}\eta, \tag{7}$$

where $I(R)$ is the Sersic intensity profile; $\eta = r/R_{\rm e}$, $M_{\rm e}$ and $\rho_\star^{\rm e}$ are the total mass and the stellar density at $R_{\rm e}$; $\Upsilon_\star$ is the stellar M/L ratio; $M_{\rm tot}(\eta)$ is the total mass, $K(\eta/\xi)$ is a kernel function depending on the choice of the anisotropy profile; and the tilted quantities are normalized with respect to their values at $R_{\rm e}$. We consider only isotropic models and take the corresponding $K(\eta/\xi)$ from appendix B of Mamon & Lokas (2005). The observed quantity is then obtained by luminosity-weighting $\sigma_{\rm los}$ in a circular aperture of radius $R_{\rm ap}$. Note that, according to the SDSS survey strategy, $R_{\rm ap}$ is fixed to 1.5 arcsec so that $\xi_{\rm ap} = R_{\rm ap}/R_{\rm e}$ changes from one lens to another.

Having set the stellar component quantities from photometry and mass estimates, we are left with only one unknown parameter, namely the halo mass $M_{\rm vir}$. We find its fiducial value minimizing the merit function

$$\chi^2 = \left[\frac{\sigma_{\rm ap}^{\rm obs} - \sigma_{\rm ap}^{\rm th}(M_{\rm vir})}{\varepsilon_\sigma}\right]^2 + \left[\frac{M_{\rm E}^{\rm obs} - M_{\rm E}^{\rm th}(M_{\rm vir})}{\varepsilon_{\rm E}}\right]^2, \tag{8}$$

where, as detailed in Cardone et al. (2009), the uncertainties (ε_σ, $\varepsilon_{\rm E}$) are obtained by summing in quadrature the observational errors and the theoretical ones as derived from the propagation of uncertainties on ($M_\star$, $R_{\rm e}$). For each lens, the best-fitting value is the one minimizing $\chi^2(M_{\rm vir})$, while $1\sigma(2\sigma)$ confidence levels are obtained by solving $\Delta\chi^2(M_{\rm vir}) = \chi^2(M_{\rm vir}) - \chi^2_{\rm min} = 1.0$ (4.0).

[2] We assume a concordance ΛCDM cosmological model so that $H^2(z)/H_0^2 = \Omega_{\rm M}(1+z)^3 + (1-\Omega_{\rm M})$ with $(\Omega_{\rm M}, h) = (0.3, 0.7)$.

[3] In principle, one could have adopted a whatever functional form provided the relation $\Delta_{\rm vir}$–$c_{\rm vir}$ is adjusted in such a way that the approximated density profile still fits the numerical one. For this reason, one has not to update the $c_{\rm vir}$–$M_{\rm vir}$ relation to account for a different cosmology or redshift. In particular, should one consider systems with $z > 0$, one must still use equation (3) without scaling $c_{\rm vir}$ by $(1+z)^{-1}$ as usually done in literature.

In order to select only the lenses with a higher significance of the model fit, one can roughly set a threshold on the reduced χ^2 values. For our best-fitting models, these are typically smaller than 1 (for 1 degree of freedom – two observational constraints versus one model parameter) mainly because the inclusion of theoretical errors on $(\varepsilon_\sigma, \varepsilon_{\rm E})$.[4] We have therefore decided to be conservative and define the splitting of the sample on the basis of their observed uncertainties rather than the significance of the fit, and define a *full* (F), a *good* (G) and the *best* (B) sample as follows.

The sample F contains all the 59 lenses. The G sample is made out of 51 lenses with the halo mass in the range of $11 \leq \log M_{\rm vir} \leq 14$ and the best-fitting values for $(\sigma_{\rm ap}, M_{\rm E})$ satisfying

$$-2.0 \leq (\sigma_{\rm ap}^{\rm obs} - \sigma_{\rm ap}^{\rm bf})/\varepsilon_\sigma \leq 2.0,$$

$$-2.0 \leq (M_{\rm E}^{\rm obs} - M_{\rm E}^{\rm bf})/\varepsilon_{\rm E} \leq 2.0.$$

The B sample is the most conservative one being made out of 46 lenses with mass in the same range, but with the following quality parameters:

$$-1.0 \leq (\sigma_{\rm ap}^{\rm obs} - \sigma_{\rm ap}^{\rm bf})/\varepsilon_\sigma \leq 1.0,$$

$$-1.0 \leq (M_{\rm E}^{\rm obs} - M_{\rm E}^{\rm bf})/\varepsilon_{\rm E} \leq 1.0.$$

The overall agreement of the best-fitting values of $(\sigma_{\rm ap}, M_{\rm E})$ with the observed ones is always quite good with rms $(1 - \sigma_{\rm ap}^{\rm bf}/\sigma_{\rm ap}^{\rm obs}) \simeq$ 7 per cent (5 per cent) and rms $(1 - M_{\rm E}^{\rm bf}/M_{\rm E}^{\rm obs}) \simeq 13$ per cent (9 per cent) for sample F (B). As a consequence, most of the results we will discuss in the following are quantitatively (within the errors) independent of the sample adopted, thus we will refer to sample G as the trade-off between fit quality and improved statistics.

Looking more closely to the galaxy filling the F sample (i.e. the bottom rows of Table 1), they mainly differ from the G sample for their higher $\log M_{\rm vir}$, exceeding the imposed limit of $10^{14}\,{\rm M}_\odot$ fulfilled by samples B and G. This has been set as an upper limit for virial masses of typical galaxy systems, and also to match the range of validity of our analytical approximation of the SIM model (see Section 2).

Such a large $\log M_{\rm vir}$ model estimates might be a warning about the accuracy of the approximation adopted to convert the SIM density profile in the one-parameter generalized NFW which tend to overestimate the virial masses. We have checked though that all (but one) of the seven most massive systems filling the F sample reside in overdense regions (following the definition adopted in Treu et al. 2009) so that we cannot exclude the inference that this mass excess in the final virial mass estimate is real and given by the contribution of the cluster itself which we cannot constrain with our limited data and is beyond the purpose of this analysis. Finally, these systems turn out to have unreasonably large virial masses even if we would use the NFW rather than the SIM model (see later). Thus, we can confidently conclude that they might not represent a critical issue specifically for the SIM model, but rather that the lensing model is missing some external field to be tracked with forthcoming more accurate analyses. To be conservative, in the following, we will exclude these very massive systems in all the scaling relation estimates.

Since we have only two observed quantities for each lens, we expect to determine $M_{\rm vir}$ on a case-by-case basis with some large uncertainty (see e.g. Table 1). In fact, according to the standard propagation of errors, most of the mass-related quantities (such as the DM mass fraction and the column densities) will be known with poor precision. As a possible way out, one could try to improve the constraints by binning the galaxies according to luminosity or stellar mass and then fitting for a parameter which is assumed to be the same for all the objects in the same bin (e.g. Cardone et al. 2009). Unfortunately, this is not possible here because of the non-universality of the DM mass profile. Indeed, since $M_{\rm vir}$ is obviously different from one lens to another, the slope γ and the concentration $c_{\rm vir}$ will differ too so that the objects in the same bin would have intrinsically different properties. As a consequence, we do not attempt any binning and prefer to deal with large error bars rather than introducing possible systematics in the analysis.

3.1 SIM versus NFW and Burkert models

The above analysis has demonstrated that the proposed SIM model is able to fit the observed aperture velocity dispersion and projected mass within the Einstein radius for the SLACS lenses sample with a reasonable significance. One might want to check whether other 'standard' halo density recipes can do a comparable job. We have commented in Section 2 that our SIM model, because of the dependence of the central slope on the virial mass, is able to match a wide range of core behaviour from 'cuspy' NFW to 'cored' Burkert models. It is then interesting to compare the best-fitting results to $(\sigma_{\rm ap}, M_{\rm E})$ as done in Section 3 and see whether data are able to favour one model with respect to the other.

We need to first remark that the main difference among these three models is that NFW and Burkert density profiles are intrinsically biparametric (although there is a correlation between the two parameters in both cases; see Section 3.1.2) while SIM is monoparametric by definition. According to Ockham's razor principle, this is an important argument to take into account in our final considerations.

3.1.1 SIM versus two-parameter NFW and Burkert profiles

The two parameters of the NFW and Burkert profiles can be similarly recast in terms of the virial mass $M_{\rm vir}$ and the concentration[5] $c = R_{\rm vir}/R_{\rm s}$ where $R_{\rm s}$ is the radius where the slope of the logarithmic density equals -2 in the NFW case and the core radius in the Burkert one. Since we have only two observed quantities for each lens, it is not possible to determine both $(c, M_{\rm vir})$ on a case-by-case basis, so that we must rely on a different strategy. We use the results from CT10, where we have therefore binned the SLACS lenses in 10 luminosity bins and expressed $(c, M_{\rm vir})$ in terms of quantities that can be assumed to be equal for all lenses in the same bin. The parameters $(c, M_{\rm vir})$ are then determined a posteriori for each single lens on the basis of the χ^2 minimization adopted in Section 3.

Both the NFW and Burkert models fit well the lens data, although, as discussed in CT10, the Burkert model leads to quite small virial

[4] It is worth noting that such a noise term can be hardly reduced. To understand why, let us consider the case of the projected mass which is the sum of the stellar and DM terms. The stellar term is proportional to the total stellar mass and hence is known with an uncertainty obtained by propagating those on the luminosity and the stellar M/L ratio. This latter is actually the major source of uncertainty in the final budget and cannot be reduced unless one rederive the estimate of $\Upsilon_\star$ relying on a larger set of colours than the one used by the SLACS collaboration.

[5] Actually, the *concentration* definition strictly applies to the NFW case. We decided to redefine it for the Burkert model for convenience, although we do not assume that this has a defined physical meaning.

Table 1. Main stellar and DM quantities of the lens ETG sample adopted. We first show the lenses of the B sample, then the ones to be added to get the G and F samples. Stellar parameters are from the SLACS collaboration (A+09), while DM quantities are derived by our best-fitting SIM model to the data. Columns are as follows: 1. galaxy ID; 2. V-band luminosity L_V; 3. logarithm of $R_{\rm e}$; 4. logarithm of the total stellar mass as taken from A+09 (assuming a Salpeter IMF); 5. model virial mass; 6. 3D DM mass fraction; 7. logarithm of the DM column density $\mathcal{S}_{\rm DM}(R_{\rm e})$; 8. logarithm of DM acceleration; 9. logarithm of the Newtonian stellar acceleration. All the quantities are given with their 1σ errors except for $\log L_V$ and $\log R_{\rm e}$ that have negligible uncertainties.

Lens ID	$\log L_V$ ($\log \mathrm{L}_\odot$)	$\log R_{\rm e}$ (kpc)	$\log M_\star$ ($\log \mathrm{M}_\odot$)	$\log M_{\rm vir}$ ($\log \mathrm{M}_\odot$)	$f_{\rm DM}(R_{\rm e})$	$\log \mathcal{S}_{\rm DM}(R_{\rm e})$ ($\mathrm{M}_\odot\,\mathrm{pc}^{-2}$)	$\log g_{\rm DM}(R_{\rm e})$ ($\mathrm{m\,s}^{-2}$)	$\log g_\star(R_{\rm e})$ ($\mathrm{m\,s}^{-2}$)
SDSSJ0008−0004	11.11	1.01	11.64 ± 0.14	12.96 ± 0.63	0.46 ± 0.16	3.16 ± 1.10	-9.67 ± 0.20	-9.63 ± 0.14
SDSSJ0029−0055	10.98	0.97	11.58 ± 0.13	13.21 ± 0.84	0.40 ± 0.19	3.10 ± 0.098	−9.69 ± 0.32	−9.60 ± 0.13
SDSSJ0037−0942	11.16	0.94	11.73 ± 0.06	13.67 ± 0.30	0.37 ± 0.18	3.17 ± 0.10	−9.53 ± 0.28	−9.38 ± 0.06
SDSSJ0157−0056	11.25	0.87	11.74 ± 0.10	13.11 ± 0.68	0.29 ± 0.14	3.18 ± 0.19	−9.61 ± 0.26	−9.24 ± 0.10
SDSSJ0216−0813	11.43	1.15	12.03 ± 0.07	13.90 ± 0.33	0.49 ± 0.20	3.23 ± 0.16	−9.42 ± 0.25	−9.51 ± 0.07
SDSSJ0252+0039	10.85	0.76	11.46 ± 0.13	11.96 ± 1.1	0.17 ± 0.09	3.05 ± 2.21	−10.00 ± 0.21	−9.30 ± 0.13
SDSSJ0330−0020	11.07	0.88	11.58 ± 0.09	12.95 ± 0.49	0.36 ± 0.11	3.06 ± 0.14	−9.66 ± 0.16	−9.41 ± 0.09
SDSSJ0728+3835	11.04	0.83	11.69 ± 0.12	12.19 ± 0.96	0.17 ± 0.08	2.92 ± 0.36	−9.92 ± 0.19	−9.21 ± 0.12
SDSSJ0819+4534	10.86	0.96	11.40 ± 0.08	13.79 ± 0.27	0.60 ± 0.21	3.22 ± 0.59	−9.45 ± 0.25	−9.75 ± 0.08
SDSSJ0822+2652	11.09	0.97	11.69 ± 0.13	13.55 ± 0.64	0.40 ± 0.21	3.16 ± 0.27	−9.57 ± 0.33	−9.48 ± 0.13
SDSSJ0903+4116	11.34	1.09	11.84 ± 0.14	12.83 ± 0.74	0.40 ± 0.15	3.13 ± 0.52	−9.74 ± 0.20	−9.58 ± 0.14
SDSSJ0936+0913	11.04	0.90	11.68 ± 0.12	12.93 ± 0.76	0.29 ± 0.13	3.21 ± 3.04	−9.73 ± 0.22	−9.36 ± 0.12
SDSSJ0946+1006	10.95	1.0	11.59 ± 0.12	13.91 ± 0.40	0.55 ± 0.22	3.22 ± 0.143	−9.42 ± 0.28	−9.64 ± 0.12
SDSSJ0959+0410	10.44	0.53	11.15 ± 0.06	13.43 ± 0.37	0.27 ± 0.13	3.16 ± 0.13	−9.53 ± 0.27	−9.15 ± 0.06
SDSSJ1016+3859	10.81	0.67	11.48 ± 0.12	13.44 ± 1.0	0.24 ± 0.17	3.24 ± 0.13	−9.54 ± 0.38	−9.11 ± 0.12
SDSSJ1020+1122	11.13	0.81	11.80 ± 0.12	13.12 ± 0.77	0.20 ± 0.12	3.14 ± 0.65	−9.66 ± 0.29	−9.06 ± 0.12
SDSSJ1023+4230	10.92	0.82	11.57 ± 0.12	13.47 ± 0.61	0.31 ± 0.18	3.18 ± 0.65	−9.58 ± 0.32	−9.30 ± 0.12
SDSSJ1112+0826	11.12	0.88	11.73 ± 0.08	14.00 ± 0.34	0.43 ± 0.20	3.31 ± 0.14	−9.31 ± 0.26	−9.27 ± 0.08
SDSSJ1134+6027	10.81	0.76	11.51 ± 0.12	13.32 ± 0.87	0.27 ± 0.17	3.17 ± 0.12	−9.61 ± 0.35	−9.24 ± 0.12
SDSSJ1142+1001	10.96	0.89	11.55 ± 0.08	13.37 ± 0.46	0.36 ± 0.17	3.13 ± 0.12	−9.62 ± 0.28	−9.44 ± 0.08
SDSSJ1153+4612	10.70	0.64	11.33 ± 0.13	13.40 ± 0.75	0.27 ± 0.17	3.21 ± 0.131	−9.55 ± 0.35	−9.19 ± 0.13
SDSSJ1205+4910	11.1	0.96	11.72 ± 0.06	13.76 ± 0.28	0.43 ± 0.19	3.21 ± 0.10	−9.46 ± 0.26	−9.43 ± 0.06
SDSSJ1218+0830	10.98	0.95	11.59 ± 0.08	13.39 ± 0.42	0.41 ± 0.17	3.09 ± 0.09	−9.65 ± 0.26	−9.56 ± 0.08
SDSSJ1306+0600	10.82	0.84	11.43 ± 0.08	13.92 ± 0.28	0.54 ± 0.19	3.28 ± 0.12	−9.32 ± 0.22	−9.48 ± 0.08
SDSSJ1313+4615	10.94	0.82	11.58 ± 0.08	13.75 ± 0.37	0.38 ± 0.19	3.23 ± 0.12	−9.44 ± 0.29	−9.30 ± 0.08
SDSSJ1318−0313	11.14	1.20	11.67 ± 0.090	13.47 ± 0.32	0.59 ± 0.19	3.12 ± 0.29	−9.70 ± 0.26	−9.96 ± 0.09
SDSSJ1402+6321	11.13	0.94	11.79 ± 0.060	13.38 ± 0.44	0.30 ± 0.15	3.12 ± 0.18	−9.65 ± 0.27	−9.33 ± 0.06
SDSSJ1403+0006	10.82	0.77	11.44 ± 0.08	13.10 ± 0.83	0.29 ± 0.14	3.11 ± 0.11	−9.67 ± 0.29	−9.34 ± 0.08
SDSSJ1416+5136	11.02	0.79	11.64 ± 0.08	13.23 ± 0.57	0.25 ± 0.12	3.14 ± 0.10	−9.61 ± 0.26	−9.17 ± 0.08
SDSSJ1430+4105	11.27	1.07	11.93 ± 0.11	13.86 ± 0.50	0.44 ± 0.21	3.22 ± 0.30	−9.44 ± 0.30	−9.44 ± 0.11
SDSSJ1436−0000	11.17	1.10	11.69 ± 0.09	13.29 ± 0.41	0.49 ± 0.16	3.12 ± 0.57	−9.70 ± 0.23	−9.75 ± 0.09
SDSSJ1451−0239	10.84	0.77	11.39 ± 0.06	13.44 ± 0.37	0.35 ± 0.15	3.12 ± 0.11	−9.59 ± 0.26	−9.39 ± 0.06
SDSSJ1525+3327	11.44	1.23	12.02 ± 0.09	13.29 ± 0.63	0.42 ± 0.19	3.16 ± 1.21	−9.74 ± 0.29	−9.68 ± 0.09
SDSSJ1531−0105	11.12	0.96	11.68 ± 0.09	13.84 ± 0.36	0.47 ± 0.20	3.22 ± 0.25	−9.44 ± 0.27	−9.48 ± 0.09
SDSSJ1538+5817	10.64	0.6	11.28 ± 0.08	12.89 ± 0.57	0.23 ± 0.08	2.99 ± 0.13	−9.67 ± 0.17	−9.15 ± 0.08
SDSSJ1614+4522	10.82	0.94	11.47 ± 0.12	12.66 ± 0.70	0.42 ± 0.13	3.06 ± 1.82	−9.79 ± 0.16	−9.65 ± 0.12
SDSSJ1621+3931	11.15	1.03	11.70 ± 0.07	13.53 ± 0.34	0.44 ± 0.18	3.14 ± 0.18	−9.61 ± 0.27	−9.59 ± 0.07
SDSSJ1627−0053	11.01	0.84	11.70 ± 0.09	13.63 ± 0.51	0.31 ± 0.17	3.20 ± 0.13	−9.50 ± 0.31	−9.23 ± 0.09
SDSSJ1630+4520	11.15	0.90	11.86 ± 0.07	13.08 ± 0.50	0.24 ± 0.09	3.06 ± 0.18	−9.68 ± 0.19	−9.18 ± 0.07
SDSSJ1636+4707	10.99	0.83	11.63 ± 0.08	12.69 ± 0.6	0.25 ± 0.08	2.98 ± 0.41	−9.74 ± 0.16	−9.26 ± 0.08
SDSSJ1644+2625	10.8	0.75	11.43 ± 0.08	13.51 ± 0.47	0.32 ± 0.17	3.17 ± 0.11	−9.56 ± 0.31	−9.31 ± 0.08
SDSSJ2238-0754	10.836	0.766	11.45 ± 0.06	12.94 ± 0.85	0.27 ± 0.12	3.05 ± 0.11	−9.71 ± 0.24	−9.32 ± 0.06
SDSSJ2300+0022	10.98	0.85	11.65 ± 0.07	13.85 ± 0.32	0.42 ± 0.19	3.27 ± 0.12	−9.35 ± 0.25	−9.28 ± 0.06
SDSSJ2303+1422	11.11	0.98	11.71 ± 0.06	13.66 ± 0.31	0.42 ± 0.19	3.15 ± 0.10	−9.55 ± 0.27	−9.49 ± 0.06
SDSSJ2321−0939	10.95	0.87	11.60 ± 0.08	13.53 ± 0.51	0.34 ± 0.18	3.13 ± 0.11	−9.59 ± 0.31	−9.38 ± 0.08
SDSSJ2341+0000	11.06	1.15	11.73 ± 0.08	13.25 ± 0.41	0.50 ± 0.15	3.89 ± 11.2	−9.74 ± 0.21	−9.80 ± 0.08
SDSSJ0737+3216	11.344	1.20	11.96 ± 0.07	13.93 ± 0.28	0.58 ± 0.20	3.22 ± 0.11	−9.42 ± 0.22	−9.67 ± 0.07
SDSSJ1100+5329	11.29	1.14	11.84 ± 0.07	12.93 ± 0.46	0.44 ± 0.11	3.17 ± 1.52	−9.76 ± 0.15	−9.67 ± 0.07
SDSSJ1106+5228	10.73	0.65	11.37 ± 0.06	13.90 ± 0.30	0.39 ± 0.17	3.30 ± 0.142	−9.30 ± 0.25	−9.17 ± 0.06
SDSSJ1204+0358	10.73	0.67	11.45 ± 0.060	13.67 ± 0.35	0.29 ± 0.16	3.23 ± 0.13	−9.45 ± 0.29	−9.12 ± 0.06
SDSSJ1250+0523	11.16	0.85	11.77 ± 0.07	12.27 ± 0.65	0.14 ± 0.06	3.13 ± 2.99	−9.95 ± 0.20	−9.16 ± 0.07
SDSSJ2347-0005	11.33	1.0	11.83 ± 0.08	14.00 ± 0.43	0.49 ± 0.22	3.32 ± 0.17	−9.30 ± 0.28	−9.40 ± 0.08
SDSSJ0044+0113	10.87	0.85	11.47 ± 0.09	14.22 ± 0.31	0.59 ± 0.21	3.38 ± 0.15	−9.20 ± 0.23	−9.47 ± 0.09
SDSSJ0912+0029	11.26	1.08	11.96 ± 0.07	14.05 ± 0.32	0.50 ± 0.19	3.25 ± 0.13	−9.36 ± 0.23	−9.44 ± 0.07
SDSSJ0935−0003	11.52	1.31	11.96 ± 0.07	14.54 ± 0.24	0.80 ± 0.14	3.39 ± 0.13	−9.17 ± 0.16	−9.89 ± 0.07
SDSSJ0956+5100	11.19	0.95	11.81 ± 0.08	14.09 ± 0.33	0.48 ± 0.20	3.32 ± 0.152	−9.27 ± 0.24	−9.32 ± 0.08
SDSSJ1143−0144	11.06	1.02	11.60 ± 0.09	14.15 ± 0.28	0.65 ± 0.20	3.29 ± 0.13	−9.29 ± 0.21	−9.68 ± 0.09
SDSSJ1213+6708	10.92	0.87	11.49 ± 0.09	14.20 ± 0.31	0.59 ± 0.21	3.36 ± 0.15	−9.21 ± 0.23	−9.49 ± 0.09
SDSSJ1719+2939	10.82	0.75	11.46 ± 0.08	14.05 ± 0.32	0.47 ± 0.20	3.36 ± 0.15	−9.23 ± 0.24	−9.27 ± 0.08

masses and hence unexpectedly low virial M/L values. In order to make a meaningful comparison, we use the same selection criteria defined above to define the *good* (G) and the *best* (B) samples for the NFW and Burkert fits. It turns out that the number of lenses in the G and B samples is (52, 50, 56) and (46, 25, 35) for the SIM, NFW and Burkert models, respectively. Note that the same lenses enter the G samples for SIM and NFW with only two cases excluded for the NFW model because of a larger virial mass. This is a consequence of the fact that the results from the SIM models generally fitted a range of masses (see Table 1) that, according to equation (5), correspond to $\gamma \geq 1$, i.e. more 'cuspy' systems.

On the contrary, almost all the lenses enter the G sample in the Burkert case because they have a far lower virial mass and the three missing lenses are excluded since they have $\log M_{\rm vir} \leq 11$. When one strengthens the constraint on the precision of the recovered $(\sigma_{\rm ap}, M_{\rm E})$, the SIM model becomes clearly preferred, its B sample being the richest one.

The SIM model turns out to be favoured by the AIC and BIC statistics (Liddle 2004) which measure the significance of the best fit taking into account the different number of degrees of freedom by penalizing the introduction of unnecessary parameters. These two estimators are defined respectively as

$$\mathrm{AIC} = -2\ln\mathcal{L}_{\rm max} + 2n$$

and

$$\mathrm{BIC} = -2\ln\mathcal{L}_{\rm max} + n\ln N_{\rm data},$$

where $\mathcal{L}_{\rm max}$ is the maximum likelihood value, n is the number of model parameters and $N_{\rm data}$ is the number of constraints. Assuming a Gaussian likelihood (as we have implicitly done), it is $-2\ln\mathcal{L}_{\rm max} = \chi^2_{\rm min}$, while $n = 1(2)$ for the SIM (NFW and Burkert) model with $N_{\rm data} = 2$. The SIM model turns out to have the lowest AIC and BIC values and is therefore the favoured one in comparison to the NFW and Burkert ones, although the small values of $\Delta\mathrm{AIC} = \mathrm{AIC_{SIM}} - \mathrm{AIC_{NFW}}$ and $\Delta\mathrm{BIC} = \mathrm{BIC_{SIM}} - \mathrm{BIC_{NFW}}$ make the NFW model statistically equivalent in most cases (and the Burkert model is generally excluded because of the highest values it gives).

A possible caveat is in order here. Although formally defined in the same way, the χ^2 values for the SIM, NFW and Burkert models are not fully equivalent since, for each lens, the total errors $(\epsilon_{\rm ap}, \epsilon_{\rm E})$ depend also on the adopted model because of the propagation of the uncertainties on the stellar masses and the effective radius (see CT10 for details[6]). Although such differences are actually quite small and do not impact the relative ranking of the models significantly, we have nevertheless computed the percentage best-fitting residuals and found (for the good samples lenses)

$$\mathrm{rms}\left[\left(\sigma_{\rm ap}^{\rm obs} - \sigma_{\rm ap}^{\rm th}\right)/\sigma_{\rm ap}^{\rm obs}\right] = 7,\ 13,\ 14\ \text{per cent};$$

$$\mathrm{rms}\left[\left(M_{\rm E}^{\rm obs} - M_{\rm E}^{\rm th}\right)/M_{\rm E}^{\rm obs}\right] = 12,\ 19,\ 16\ \text{per cent}$$

for SIM, NFW and Burkert models, respectively. Again, we find that the SIM model best reproduces the observed data so that we can safely argue that it should be preferred with respect to the NFW and Burkert models. This is one of the central results of this paper, since we seem to have proved that a monoparametric density profile (including most of the physics of the galaxy collapse) works better than two-parameter density profiles with a much weaker physical content (e.g. collapse and evolution of collisionless DM particles). However, this result is based on a different procedure of fitting, thus one can argue that the final significance of the fit might have been affected by the use of binned data to constraint the halo parameters. In the next section we will use the well-known correlations between the two density parameters of NFW (and Burkert) profiles to check whether their one-parameter rewriting can match the one-by-one data with similar significance.

3.1.2 SIM versus one-parameter NFW and Burkert profiles

For the NFW density profile there is a well-established correlation between the virial mass and the concentration as found in N-body simulations. Following the recent analysis in Muñoz-Cuartas et al. (2011), we therefore set

$$\log c_{\rm NFW} = a_{\rm NFW}(z)\log\left(\frac{M_{\rm vir}}{h^{-1}\,\mathrm{M}_\odot}\right) + b_{\rm NFW}(z) \tag{9}$$

with

$$a_{\rm NFW}(z) = 0.029z - 0.097,$$

$$b_{\rm NFW}(z) = -\frac{110.001}{z+16.885} + \frac{2469.720}{(z+16.885)^2},$$

for $10 \leq \log[M_{\rm vir}/(h^{-1}\,\mathrm{M}_\odot)] \leq 15$. If we ignore the scatter in equation (9) as a first approximation, this one-parameter version of the NFW model can be fitted to the SLACS lenses with the virial mass being only an unknown quantity. Using this approach, we thus find a viable solution for all the 59 objects in the sample with 53 (50) lenses satisfying the selection criteria used to define the good (best) sample for the SIM case. In particular, the quality of the fit may be quantified by noting that

$$\mathrm{rms}\ (1 - \sigma_{\rm ap}^{\rm bf}/\sigma_{\rm ap}^{\rm obs}) \simeq 4\ \text{per cent and rms}\ (1 - \mathrm{M}_{\rm E}^{\rm bf}/\mathrm{M}_{\rm E}^{\rm obs}) \simeq 13\ \text{per cent}$$

for the good sample and

$$\mathrm{rms}\ (1 - \sigma_{\rm ap}^{\rm bf}/\sigma_{\rm ap}^{\rm obs}) \simeq 4\ \text{per cent and rms}\ (1 - \mathrm{M}_{\rm E}^{\rm bf}/\mathrm{M}_{\rm E}^{\rm obs}) \simeq 11\ \text{per cent}$$

for the best one. We have repeated the same exercise with the Burkert model, by using the relation between the core density ρ_0 and the core radius r_0 found in Salucci & Burkert (2000) to reduce the density model to a one-parameter profile. Imposing this relation and fitting each single lens using the virial mass as the only parameter, we have found a viable solution for only six lenses, which suggests that a monoparametric Burkert profile is incapable of matching the SLACS data and we do not discuss this case hereafter.[7]

If we make a more detailed comparison of the SIM model to the NFW model, we will see that the latter works better in matching the aperture velocity dispersion, while the former is in a slightly better agreement with the projected mass values. Overall, however, both models match the data so well that the choice of which model is most viable should be driven by physical motivations. We indeed prefer the SIM model since the mass–central slope relation comes out from a physical model rather than being the outcome of a numerical simulation. However, this argument alone does not allow us to

[6] Summarizing, the difference between the theoretically predicted and the observed values of the velocity dispersion and the projected mass entering the χ^2 evaluation are normalized with respect to the errors, but these errors are partially model-dependent. For instance, the uncertainty on the theoretically predicted $M_{\rm proj}$ is propagated from the one on the stellar mass to a formula which depends on the adopted DM halo profile.

[7] Note, however, that this is likely a consequence of having assumed that the ρ_0–r_0 relation found at $z = 0$ applies to any z.

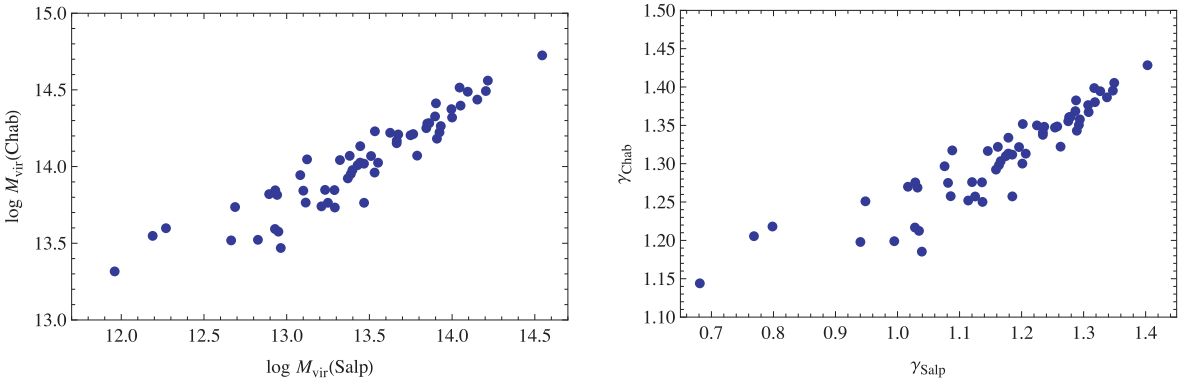

Figure 1. Best-fitting virial mass (left) and inner slope (right) for the SIM model with Salpeter (x-axis) and Chabrier IMF (y-axis).

definitely abandon other density models and as far as both SIM and one parameter NFW (as well as the two-parameter version of NFW and Burkert models, as discussed above) well reproduce the SLACS lens data, we will hereafter consider all options and will a posteriori check the difference introduced by the different models.

3.2 Changing from Salpeter to Chabrier IMF

As fiducial values for the stellar mass of each lens, we have adopted the estimates given in table 4 of Auger et al. (2010) under the assumption of a Salpeter IMF. However, since IMF is still an uncertain variable in the mass analysis, in this section we want to investigate the impact of a different IMF choice on the SIM results.

We therefore consider the case of the Chabrier (2001) IMF which returns stellar masses smaller by a factor of 1.8 with respect to the ones obtained with the Salpeter IMF. As the Chabrier IMF provides the lowest masses compatible with the colours of the galaxy, this will allow us to minimize the contribution to the velocity dispersion and projected mass by the stellar component.

As for the Salpeter IMF, it turns out that all the lenses may be well fitted with the best-fitting theoretical values of σ_{ap} and M_E within 2σ (1σ) of the observed ones for 59 (53) out of 59 lenses in the SLACS sample. Seemingly, the ability of the SIM model to fit the data is not affected by the IMF choice. However, when looking at the estimated virial masses for the Chabrier IMF case, the inferred values turned out to be generally larger (i.e. $\log M_{vir} > 14.0$) than the ones obtained by the Salpeter IMF such that only 25 (24) lenses enter the G (B) sample.

This is made clearer in Fig. 1, where we show that the best-fitting virial masses for the SIM + Chabrier model are almost 1 order of magnitude larger than those for the SIM + Salpeter case because of the lower stellar masses predicted by the Chabrier IMF which maximize the DM contribution to the central parts. This is 'seen' by the SIM model as the presence of a more cuspy profile which implies a larger γ and a larger M_{vir} according to equation (5).

Based on the argument of unrealistic virial masses, we are inclined to rule out the SIM + Chabrier model. This is however becoming a common conclusion from different analyses: e.g. gravitational lensing (see, e.g. Cardone & Tortora 2010; Treu et al. 2010) and studies of the central DM fraction in local ETGs (Napolitano et al. 2011) suggest that observations are consistent more with a Salpeter rather than a Chabrier IMF for ETGs (unless some strong AC is considered). Moreover, it has also been suggested that the IMF might vary with luminosity (Renzini & Ciotti 1993; Tortora et al. 2009) with a Salpeter one being generally preferred for brighter systems (as probed by the SLACS lenses).

4 DARK MATTER SCALING RELATIONS

Despite the large uncertainties, we have shown that the SIM halo model is able to fit the combination of galaxy kinematics and lensing data fairly well. We have also fixed the stellar mass contribution by assuming the Salpeter IMF; we can now start looking into the DM properties of the galaxy sample.

The scaling relations we are interested in are commonly written as power laws and can be conveniently converted into linear relations in a log–log space, $\log y = \log A + B \log x$, with comparable uncertainties on $(\log x, \log y)$. As a best-fitting procedure, we will follow the approach as in CT10 and adopt the Bayesian method described in D'Agostini (2005; see also Hogg, Bovy & Lang 2010).

For the scaling relations we want to examine, we need to choose a reference radius where the mass quantities are evaluated. As these estimates will imply some model extrapolation, this choice is critical since results can be strongly model-dependent.

Since our data mainly probe the region close to R_e, this seems the natural choice as the reference radius. Sometimes also the core radius R_c, introduced in the cored density models, and the same R_s where the logarithmic slope of the density profile is -2, are taken as reference radii. It is, however, easy to check that both of these quantities are far larger than R_e so that one would stay in the inconvenient position of deriving column density estimates for regions much more far away with the distance constrained by the data extension. As the proposed model has proven to match the observations around $R_e$fairly well, we will compute the scaling relations at this reference distance.

As a final remark, we stress that using M_{vir} as a model parameter allows us to avoid extrapolation of the mass estimates constrained at R_e out to the far larger virial radius, as commonly done in parametric modelling procedures. This makes our virial quantities intrinsically more robust.

4.1 Column density

We start by considering the correlations of the DM column density $\mathcal{S}_{DM}(R) = M^{proj}_{DM}(R)/\pi R^2$ with luminosity, stellar mass, effective radius and virial mass. The best-fitting relations obtained for the $\mathcal{S}_{DM}(R_e)$ are[8]

[8] Hereafter, we will discuss only the results for the sample G having checked that fully consistent constraints are obtained using the F and B samples. This can also be qualitatively seen in the figures where all the points are plotted with different symbols.

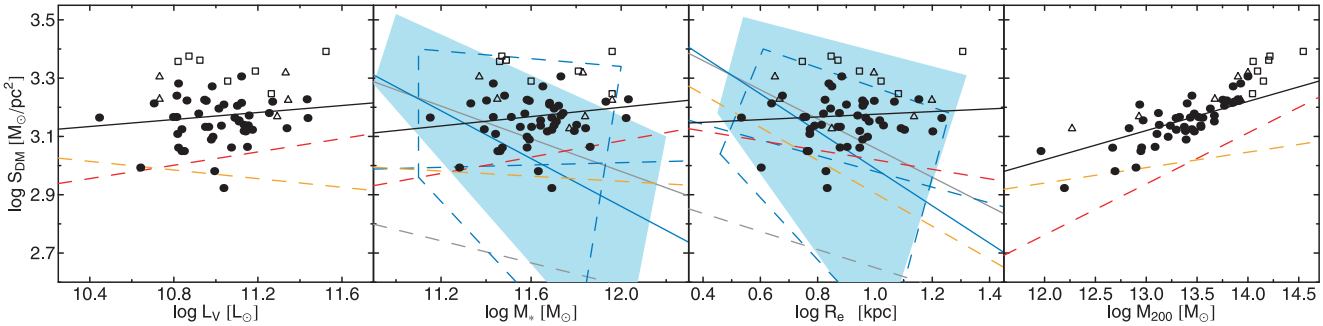

Figure 2. Best-fitting relations between the effective column density $\mathcal{S}_{\rm DM}(R_{\rm e})$ and the total luminosity L_V, stellar mass $M_\star$, effective radius $R_{\rm e}$ and halo mass M_{200} from left to right. Data in sample B are plotted as points, while the other data not present in B, but in samples G and F, are plotted as triangles and boxes, respectively. We do not plot error bars to not clutter the plot. However, typical errors are $\langle\sigma(\log M_\star)/\log M_\star\rangle \simeq 1$ per cent, $\langle\sigma(\log M_{\rm vir})/\log M_{\rm vir}\rangle \simeq 2$ per cent, $\langle\sigma(\log \mathcal{S}_{\rm DM}(R_{\rm e}))/\log \mathcal{S}_{\rm DM}(R_{\rm e})\rangle \simeq 11$ per cent, while $\log L_V$ and $\log R_{\rm e}$ have a negligible error. The continuous black line is the best fit made using sample G (i.e. points and triangles). The red and orange dashed lines are the best fit obtained in CT10, using a NFW + Salpeter IMF and a Burkert + Salpeter IMF, respectively. The continuous blue line and the cyan-shaded region are respectively the best fit and the region enclosing the data for the results in Tortora et al. (2010) using a spherical isothermal sphere, SIS (adopting a Salpeter IMF and projected quantities), while the dashed ones are for the same data but using masses in A+09. Continuous and dashed grey lines are the best fits of local ETGs in T+09, using an SIS and a constant M/L profile, respectively.

$$\log \mathcal{S}_{\rm DM}(R_{\rm e}) = 0.06 \log\left(L_{\rm V}/10^{11}\,{\rm L}_\odot\right) + 3.17,$$

$$\log \mathcal{S}_{\rm DM}(R_{\rm e}) = 0.08 \log\left(M_\star/10^{11}\,{\rm M}_\odot\right) + 3.12,$$

$$\log \mathcal{S}_{\rm DM}(R_{\rm e}) = 0.05 \log R_{\rm e} + 3.13,$$

$$\log \mathcal{S}_{\rm DM}(R_{\rm e}) = 0.10 \log\left(M_{200}/10^{12}\,{\rm M}_\odot\right) + 3.02,$$

which are also shown in Fig. 2 as compared to the individual galaxy data points. The intrinsic scatter of the fitting procedure, $\sigma_{\rm int}$, is formally negligible for all the scaling relations above and is not to be considered further on, while the true uncertainty of the fit is dominated by the data-point scatter, an issue to which we will come back later on. As a virial mass estimate we use M_{200} (i.e. the mass within the radius R_{200} where the mean density is 200 times the cosmological mean matter density) for homogeneity with previous literature studies.

Taking at face values, these relations suggest a non-universality of $\mathcal{S}_{\rm DM}(R_{\rm e})$ in agreement with what we have found in CT10 using a different halo model but the same reference radius. A similar comparison with other results in the literature is not straightforward because of differences in regard to the models adopted, the radius where $\mathcal{S}_{\rm DM}(R)$ is evaluated for each individual system, and finally the galaxy sample considered, e.g. using an NFW halo profile, B09 found a strong correlation between $\mathcal{S}_{\rm DM}(R_{\rm s})$ and the halo mass over a wide range of masses, ranging from dwarf spheroidal galaxies to galaxy clusters. On the contrary, Donato et al. (2009, hereafter D09) using the Burkert (1995, B95 hereafter) profile found a remarkably constant $\mathcal{S}_{\rm DM}(R_{\rm c})$ ($R_{\rm c}$ being the core radius of the B95 model) with the luminosity on a sample of local spirals and ellipticals. These 'cored' profiles are in contrast, though, with our SIM model which has no core but an inner cusp. Furthermore, as shown in CT10, an inconvenience with the B95 model is that it does not allow a decent fit to the SLACS data unless one assumes unreasonably low values of the virial M/L ratio. Our lens systems, instead, is made of (mainly) ETGs at an intermediate z, thus partially overlapping with B09 and completely complementary to the D09 sample. For these systems, we cannot exclude the possibility that some of the discrepancies with the results above can be applied to some evolution with the redshift of the slope of the $\mathcal{S}_{\rm DM}(R_{\rm e})$ versus (L_V, $M_\star$, $R_{\rm e}$, M_{200}). Although not investigated in detail elsewhere (but see, e.g. B09 and NRT10 for some hints), the galaxy morphology can be another important reason responsible for the discrepancies in the scaling correlations above. Our data are therefore not the best to solve the differences between B09 and D09 contrasting results; however, they might provide a benchmark result for the correlations expected of ETGs under a generalized halo model with no fixed cuspy density profile (somehow covering the intermediate range between the B95 and the NFW central behaviour).

This is particularly true due to the uncertainties in the slope and zero-point of the fitted relations. Although we use a robust Bayesian fitting method, the confidence regions around the parameter fit are large (see Table 2) due to the large error bars on the DM-related quantities. Such uncertainties make any assessment on the non-universality of the relations rather weak. Indeed, considering the 68 per cent confidence ranges, a zero value for the slope can be statistically excluded only for the $\mathcal{S}_{\rm DM}(R_{\rm e})$–$M_{200}$ relation, which is however consistent with zero within 95 per cent confidence level (CL).

Thus, looking at the correlations with the stellar quantities ($R_{\rm e}$, M_*, L_V), the $\mathcal{S}_{\rm DM}(R_{\rm e})$ universality cannot be ruled out. On the other hand, the strong correlation with the halo mass M_{200} in Fig. 2 works against the $\mathcal{S}_{\rm DM}(R_{\rm e})$ universality. This might be one reason for the contrasting results between D09 and B09: in fact the former show the absence of a trend of column density with luminosity, while the latter show a strong trend with halo mass, which is along the line of our conclusions.

However, even if we look at the correlations with luminosity, we are inclined to argue that the claim of a constant $\mathcal{S}_{\rm DM}(R_{\rm e})$ with luminosity is motivated for the later type galaxies, while the ETGs have an intrinsically larger scatter (see also NRT10) which is the effect of a stronger correlation with the halo mass (see also Section 4.2).

Focusing on the difference produced by the adoption of the different halo profiles, we can now compare the results obtained with the SIM model with findings in recent literature using the same IMF and SLACS data set.

CT10 have found lower average DM column densities over the sample, $\Delta \log \mathcal{S}_{\rm DM}(R_{\rm e}) \sim 0.1$–$0.3$, with respect to the one obtained with the SIM. This is due to the fact that the SIM model has an average central slope, $\gamma \sim 1.0$–1.3, which is steeper than the one of

Table 2. Constraints on the slope and the zero-point of the correlations involving $\mathcal{S}_{\rm DM}(R_{\rm e})$, $\mathcal{S}_{\rm tot}$, $g_{\rm DM}$ and $g_\star$ using the sample G. For each parameter, we report the best fit, mean and median values and the 68 and 95 per cent confidence ranges. Results from the fit to the other samples are fully consistent so that we will not report them, but make them available on request.

Fit	Slope					Zero-point				
	$x_{\rm BF}$	$\langle x\rangle$	$x_{\rm med}$	68 per cent CL	95 per cent CL	$x_{\rm BF}$	$\langle x\rangle$	$x_{\rm med}$	68 per cent CL	95 per cent CL
$\mathcal{S}_{\rm DM}(R_{\rm e})$–$L_V$	0.06	0.02	0.02	(−0.09, 0.14)	(−0.16, 0.23)	3.1670	3.1671	3.1682	(3.1631, 3.1694)	(3.1597, 3.1729)
$\mathcal{S}_{\rm DM}(R_{\rm e})$–$M_\star$	0.08	0.06	0.07	(−0.04, 0.17)	(−0.16, 0.28)	3.1204	3.1228	3.1157	(3.0740, 3.1782)	(2.9801, 3.2478)
$\mathcal{S}_{\rm DM}(R_{\rm e})$–$R_{\rm e}$	0.05	0.07	0.07	(−0.04, 0.19)	(−0.17, 0.30)	3.1257	3.0788	3.0506	(3.0117, 3.1882)	(2.9229, 3.2960)
$\mathcal{S}_{\rm DM}(R_{\rm e})$–$M_{200}$	0.10	0.10	0.10	(0.05, 0.16)	(−0.02, 0.21)	3.0189	2.9892	2.9615	(2.9294, 3.0745)	(2.8660, 3.1560)
$\mathcal{S}_{\rm tot}$–L_V	−0.17	−0.19	−0.19	(−0.27, −0.11)	(−0.37, −0.02)	3.4390	3.4344	3.4364	(3.4253, 3.4394)	(3.4245, 3.4424)
$\mathcal{S}_{\rm tot}$–$M_\star$	−0.16	−0.16	−0.16	(−0.24, −0.07)	(−0.34, 0.02)	3.5390	3.5207	3.5144	(3.4777, 3.5747)	(3.4353, 3.6331)
$\mathcal{S}_{\rm tot}$–$R_{\rm e}$	−0.37	−0.34	−0.33	(−0.45, −0.24)	(−0.59, −0.13)	3.7635	3.7391	3.7487	(3.6724, 3.8000)	(3.5613, 3.9340)
$\mathcal{S}_{\rm tot}$–M_{200}	0.01	0.01	0.01	(−0.06, 0.08)	(−0.12, 0.16)	3.4469	3.3381	3.3760	(3.1088, 3.5102)	(3.1013, 3.6076)
$g_{\rm DM}$–L_V	−0.04	−0.02	−0.01	(−0.17, 0.12)	(−0.30, 0.28)	−9.628	−9.625	−9.626	(−9.631, −9.615)	(−9.635, −9.614)
$g_{\rm DM}$–$M_\star$	−0.03	0.00	−0.01	(−0.14, 0.13)	(−0.29, 0.29)	−9.607	−9.621	−9.611	(−9.702, −9.550)	(−9.777, −9.441)
$g_{\rm DM}$–$R_{\rm e}$	−0.04	0.03	0.03	(−0.12, 0.18)	(−0.33, 0.35)	−9.590	−9.637	−9.625	(−9.771, −9.535)	(−9.921, −9.332)
$g_{\rm DM}$–M_{200}	0.25	0.24	0.24	(0.17, 0.30)	(0.10, 0.37)	−9.947	−9.978	−9.961	(−10.130, −9.864)	(−10.145, −9.770)
$g_\star$–L_V	−0.42	−0.38	−0.38	(−0.51, −0.26)	(−0.63, −0.13)	−9.394	−9.395	−9.395	(−9.397, −9.394)	(−9.399, −9.391)
$g_\star$–$M_\star$	−0.35	−0.28	−0.28	(−0.41, −0.14)	(−0.58, 0.08)	−9.180	−9.217	−9.191	(−9.287, −9.179)	(−9.422, −9.066)
$g_\star$–$R_{\rm e}$	−1.03	−1.02	−1.02	(−1.12, −0.92)	(−1.24, −0.80)	−8.475	−8.455	−8.428	(−8.529, −8.426)	(−8.647, −8.334)
$g_\star$–M_{200}	−0.07	−0.07	−0.08	(−0.15, 0.00)	(−0.25, 0.10)	−9.308	−9.305	−9.306	(−9.378, −9.231)	(−9.527, −9.091)

the NFW and implies a projected DM mass within $R_{\rm e}$ larger than the one obtained with the same NFW.

However, the slope of the $\mathcal{S}_{\rm DM}(R_{\rm e})$ versus $(L_V, M_\star, M_{200})$ correlations stay very similar for the two halo models (see solid black and red dashed lines in Fig. 2)[9] which means that the details of the central DM density are possibly insensitive to the global quantities. On the contrary, the $\mathcal{S}_{\rm DM}(R_{\rm e})$ seems much more sensitive to the scale of the luminous matter as the slope of the $\mathcal{S}_{\rm DM}(R_{\rm e})$–$R_{\rm e}$ correlation is inverted with respect to NFW. In particular, from Fig. 2, we see that NFW produces almost similar $\mathcal{S}_{\rm DM}(R_{\rm e})$ for smaller $R_{\rm e}$ (red dashed line) which means that the two density profiles are very similar for more compact objects, while it clearly produces a much smaller DM column density at a larger $R_{\rm e}$, where the SIM model accommodates the steeper slopes. Despite the low significance of the trend, this is a key result of our analysis because this points to a correlation between the halo central slope and the size of the luminous matter in the sense that bigger galaxies are formed in more cuspy haloes. This is qualitatively consistent with what has already been found in DP09 and Del Popolo & Kroupa (2009), which have suggested that more massive haloes are cuspier. As a side note, the presence of steeper cusps for massive systems goes in the same direction of the effect expected of the canonical AC which seems to be necessary to model extended kinematics, e.g. using planetary nebulae as mass tracers, in massive ETGs (Napolitano et al. 2011) and not in more regular ones (Napolitano et al. 2009). If so, the steeper cusps would reduce the strength of the actual AC recipe with respect to the classical prescriptions (Blumenthal et al. 1986; Gnedin et al. 2004) as reported elsewhere.

[9] We note that in particular the correlation with M_{200} might look somewhat too shallow to an eyeball check. We have checked that if we use the sample F, the best-fitting slope increases to 0.13 which is closer to the 0.17 value found when the NFW model is used (red dashed) similarly to the correlation found with L_V and $M_\star$. Moreover, a steeper slope could be found by excluding the least massive points, although there seems to be nothing unusual for these lenses to be reasonably excluded here and not elsewhere.

For a comparison with more general mass profiles, T+10 adopted a singular isothermal model to describe the stellar + DM mass profile. Here the difference is that the stellar masses have been derived using different population models. The solid blue lines in the two middle panels of Fig. 2 show that their $\mathcal{S}_{\rm DM}(R_{\rm e})$–$M_\star$ and $\mathcal{S}_{\rm DM}(R_{\rm e})$–$R_{\rm e}$ relations have the opposite trend of the one we have found from the SIM. Note that a decreasing $\mathcal{S}_{\rm DM}(R_{\rm e})$ with both the stellar mass and the effective radius is also found by T+09 for local ETGs, adopting the same mass model and stellar population properties (grey continue line in Fig. 2), but fitting very central velocity dispersions. A similar (albeit shallower) decreasing trend and lower average column densities [of $\Delta \log \mathcal{S}_{\rm DM}(R_{\rm e}) \sim 0.3$–$0.5$] are also found from T+10 for a model with a constant M/L model (grey dashed line in Fig. 2).

As T+10 do not assume a halo density profile, but derive the DM mass by subtraction of the stellar component from the total density profile, their approach seems much more dependent on the stellar population analysis (i.e. IMF, priors on stellar population parameters, availability of photometric or spectral data, etc.), e.g. while stellar masses in T+10 are, on average, consistent with the ones from A+09, some tilt is present and finally propagates to a different final estimate of $\mathcal{S}_{\rm DM}(R_{\rm e})$. Indeed, adopting the same total mass model, but the A+09 masses, the $\mathcal{S}_{\rm DM}(R_{\rm e})$–$M_\star$ correlation changes its sign, while the $\mathcal{S}_{\rm DM}(R_{\rm e})$–$R_{\rm e}$ one becomes shallower so that the disagreement with our SIM-based results is partially alleviated.[10] This check is a warning to us about the importance of the mass model and stellar population analysis adopted which, in principle, is an important player in the definition of the DM scaling relations.

Keeping this in mind, we decided to check the scaling relations of the total column density $\mathcal{S}_{\rm tot}$ (obtained including the stellar mass within $R_{\rm e}$) obtained with the SIM model for our particular stellar

[10] Note that the results obtained in T+10, using the two stellar mass sets, populate similar regions in the space $\mathcal{S}_{\rm DM}(R_{\rm e})$–$M_\star$ and $\mathcal{S}_{\rm DM}(R_{\rm e})$–$R_{\rm e}$ (see the cyan region and the one enclosed within the blue lines in Fig. 2).

population and IMF choice. As the best-fitting correlations we find

$$\log \mathcal{S}_{\rm tot} = -0.17 \log \left(L_V/10^{11}\,{\rm L}_\odot\right) + 3.44,$$

$$\log \mathcal{S}_{\rm tot} = -0.16 \log \left(M_\star/10^{11}\,{\rm M}_\odot\right) + 3.54,$$

$$\log \mathcal{S}_{\rm tot} = -0.37 \log R_{\rm e} + 3.74,$$

$$\log \mathcal{S}_{\rm tot} = 0.01 \log \left(M_{200}/10^{12}\,{\rm M}_\odot\right) + 3.34,$$

whose marginalized constraints on the slopes and the zero-points are given in Table 2. A zero slope is excluded at the 68 per cent CL for $\mathcal{S}_{\rm tot}$ versus (L_V, $M_\star$, $R_{\rm e}$) correlations, while we do not find any correlation with M_{200}. Thus, the net effect of the inclusion of the stellar component is to tilt the trend almost uniformly clockwise towards more negative slopes (and contemporary increase the zero-point due to the addition of the stellar mass). In fact, we have checked that the slope in the central regions of our light profiles become shallower at larger $R_{\rm e}$, possibly combining with the DM slope the results above. One of the possible drivers of such trends is galaxy merging, which has been shown to produce shallower slopes in simulated haloes (e.g. Boylan-Kolchin & Ma 2004). The trend of the $\mathcal{S}_{\rm tot}$ seems consistent with the recent finding from Auger et al. (2010) who, adopting a simple power-law density to shape the full mass profile of the SLACS lenses, have found a strong inverse correlation of the total density slope with $R_{\rm e}$.

4.2 Newtonian acceleration

The issue of the universality of the column density $\mathcal{S}_{\rm DM}(R)$ has some important dynamical consequences if one considers that it can be easily related to the Newtonian acceleration $g_{\rm DM}(r) = GM_{\rm DM}(r)/r^2$ (Gentile et al. 2009, hereafter G09). In particular, G09 have shown evidences for the universality of both $g_{\rm DM}(R_{\rm c})$ and $g_\star(R_{\rm c})$ with the label *DM* ($\star$) referring to DM (stellar) quantities, over a (small) sample of spirals and ellipticals. Let us first discuss the DM case evaluating the acceleration at the effective radius to be consistent with our choice throughout the paper. For the best-fitting relations (plotted in Fig. 3), we get

$$\log g_{\rm DM}(R_{\rm e}) = -0.04 \log \left(L_V/10^{11}\,{\rm L}_\odot\right) - 9.63,$$

$$\log g_{\rm DM}(R_{\rm e}) = -0.03 \log \left(M_\star/10^{11}\,{\rm M}_\odot\right) - 9.61,$$

$$\log g_{\rm DM}(R_{\rm e}) = -0.04 \log R_{\rm e} - 9.60,$$

$$\log g_{\rm DM}(R_{\rm e}) = 0.25 \log \left(M_{200}/10^{12}\,{\rm M}_\odot\right) - 9.95,$$

where the accelerations are in the units of m s^{-2}. Similarly to the column densities, we find that the DM Newtonian acceleration has no correlation with the stellar quantities (L_V, $M_\star$, $R_{\rm e}$), while it strongly correlates with M_{200}. Thus we confirm that $g_{\rm DM}$ is a constant with respect to the stellar quantities although it is larger than the value found by G09 for the $g_{\rm DM}$ computed at $R_{\rm c}$. The latter is an upper limit to our $R_{\rm e}$ estimates since generally $R_{\rm c} \gtrsim R_{\rm e}$ and for a given constant core density ρ_0 the Newtonian acceleration scales linearly with radius, i.e. $g_{\rm DM}(R_{\rm e}) \lesssim g_{\rm DM}(R_{\rm c})$. As already noted by NRT10, this result works against the universality of the $g_{\rm DM}$, which instead seems to scale with the morphological type (and possibly the mass).

The SIM estimates obtained here are discrepant with the results from CT10 for the NFW and B95 (Fig. 3). In particular our $g_{\rm DM}$ are located in between the two reference halo models, while the difference in the slopes with all the quantities are statistically insignificant. This result is somehow different with respect to the $\mathcal{S}_{\rm DM}(R_{\rm e})$ in Fig. 2 where the CT10 estimates are almost everywhere lower than the SIM estimates, which might be traced to the fact that here we have considered 3D quantities. In particular, the large values obtained by CT10 for the B95 are related to the fact that typical core radii in CT10 are smaller than $R_{\rm e}$ thus not representing a real cored profile, but rather better resembling a pseudo-isothermal sphere, with a rather steep slope around $R_{\rm e}$. In fact the deviations are more marked for the smaller systems which will also have shallower inner slopes (according to equation 5), and thus are overestimated by the steeper densities implied by the B95 models. On the other hand, the $g_{\rm DM}(R_{\rm e})$ are systematically larger than the values obtained in CT10 for NFW because of the steeper 3D slopes. We remark here that the 3D quantities are more weakly depending on the inner slopes with respect to the projected ones shown in Fig. 1, a fact that translates with an null correlation of the $g_{\rm DM}$ with $R_{\rm e}$.

As to the stellar Newtonian acceleration, we find the following as best-fitting relations:

$$\log g_\star(R_{\rm e}) = -0.42 \log \left(L_V/10^{11}\,{\rm L}_\odot\right) - 9.39,$$

$$\log g_\star(R_{\rm e}) = -0.35 \log \left(M_\star/10^{11}\,{\rm M}_\odot\right) - 9.18,$$

$$\log g_\star(R_{\rm e}) = -1.03 \log R_{\rm e} - 8.48,$$

$$\log g_\star(R_{\rm e}) = -0.07 \log \left(M_{200}/10^{12}\,{\rm M}_\odot\right) - 9.31,$$

which clearly demonstrate that this is not a universal quantity (and indeed the confidence ranges for the slope in Table 2 exclude a zero slope at the 68 per cent CL) in agreement with CT10. Note, however, that a correlation of $g_\star(R_{\rm e})$ with the stellar quantities (L_V, $M_\star$, $R_{\rm e}$) is expected, being all these quantities involved in its definition. On the contrary, the correlation with M_{200} is very weak, which shows

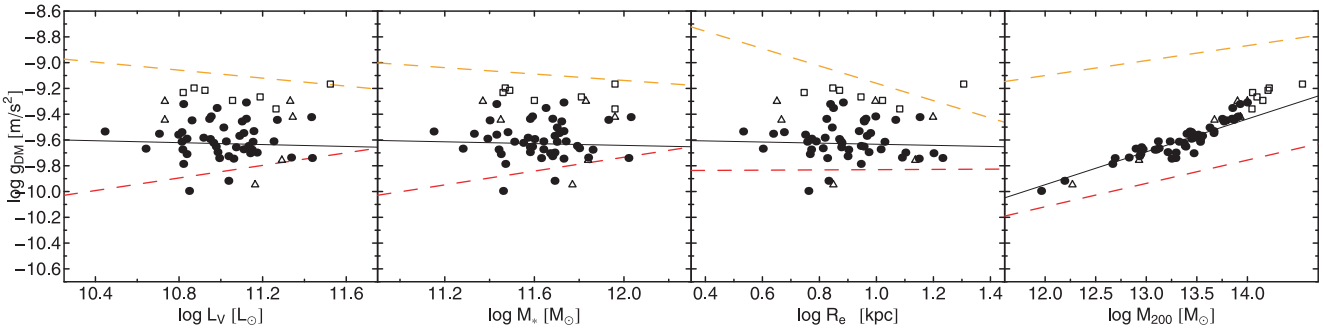

Figure 3. Best-fitting relations between the DM Newtonian acceleration (in units of m s^{-2}) and the total luminosity L_V, stellar mass $M_\star$, effective radius $R_{\rm e}$ and halo mass M_{200} from left to right. Typical error bars are $\langle \sigma[\log g_{\rm DM}(R_{\rm e})]/\log g_{\rm DM}(R_{\rm e})\rangle \simeq 2$ per cent. Symbols and lines are the same as those in Fig. 2.

that there is not any strong dependence of the stellar mass at the centres on the global DM content.

4.3 Dark matter mass content

In the previous sections we have seen that the total and DM column densities correlate differently with luminosity, stellar mass and R_e, which will depend on the different spatial distributions of stellar and dark matter. Here we want to investigate the consequences of the column density scaling relations in term of the central DM fractions. To this end, we note that

$$\frac{\mathcal{S}_{\rm DM}}{\mathcal{S}_{\rm tot}} = \frac{M_{\rm DM}^{\rm proj}(R_e)}{M_\star{}^{\rm proj}(R_e) + M_{\rm DM}^{\rm proj}(R_e)} = f_{\rm DM}^{\rm proj}(R_e),$$

where $f_{\rm DM}^{\rm proj}(R_e)$ is the projected DM fraction. Considering the best-fitting values of the correlations of both column densities with stellar parameters, we obtain that the projected DM fraction within R_e scales with the luminosity, stellar mass and R_e, as $f_{\rm DM}^{\rm proj}(R_e) \propto L_V^{0.23}$, $f_{\rm DM}^{\rm proj}(R_e) \propto M_\star{}^{0.24}$ and $f_{\rm DM}^{\rm proj}(R_e) \propto R_e{}^{0.42}$.

The same results are found by the direct fitting of the same quantities of the individual galaxies, adopting our Bayesian fitting procedure:

$$\log f_{\rm DM}^{\rm proj}(R_e) = 0.21 \log\left(L_V/10^{11}\,{\rm L}_\odot\right) - 0.21,$$

$$\log f_{\rm DM}^{\rm proj}(R_e) = 0.18 \log\left(M_\star/10^{11}\,{\rm M}_\odot\right) - 0.32,$$

$$\log f_{\rm DM}^{\rm proj}(R_e) = 0.41 \log R_e - 0.58,$$

while the 68 per cent confidence ranges of the slopes are (0.15, 0.26), (0.12, 0.24) and (0.34, 0.45) for $f_{\rm DM}^{\rm proj}$–L_V, $f_{\rm DM}^{\rm proj}$–$M_\star$ and $f_{\rm DM}^{\rm proj}$–R_e, respectively. We have therefore a clear evidence that the different scalings of $\mathcal{S}_{\rm DM}(R_e)$ and $\mathcal{S}_{\rm tot}$ with the stellar quantities are an expected consequence of the varying DM content within the effective radius.

Similarly, we define the three-dimensional DM fraction as $f_{\rm DM}(R_e) = M_{\rm DM}(R_e)/[M_\star(R_e) + M_{\rm DM}(R_e)]$ and investigate its correlation with the stellar quantities. Our best-fitting relations are

$$\log f_{\rm DM}(R_e) = 0.22 \log\left(L_V/10^{11}\,{\rm L}_\odot\right) - 0.44,$$

$$\log f_{\rm DM}(R_e) = 0.15 \log\left(M_\star/10^{11}\,{\rm M}_\odot\right) - 0.53,$$

$$\log f_{\rm DM}(R_e) = 0.59 \log R_e - 0.98,$$

while the 68 per cent CL for the slope are (0.08, 0.30), (0.02, 0.24), (0.36, 0.71), respectively. Despite the large uncertainties, these results show that brighter, more massive and bigger systems have a larger DM content within the effective radius, in qualitative agreement with previous results in literature, regardless of the adoption of deprojected or projected quantities (e.g. Padmanabhan et al. 2004; Cappellari et al. 2006; T+09; Auger et al. 2010; NRT10; T+10). We, however, note that our best-fitting relations with L_V and $M_\star$ are much shallower than what is found in CT10 for the fiducial NFW model (and Salpeter IMF), but in a good agreement with the ones in Cardone et al. (2009), where a phenomenologically motivated general halo profile was used to fit the same SLACS data considered here.

4.4 Impact of the IMF choice

All the results discussed so far have been obtained using the SIM model for the dark halo and a Salpeter IMF. As discussed in Section 3.3, choosing a Chabrier IMF leads to SIM models having a virial mass larger than $10^{14}\,{\rm M}_\odot$ for more than 50 per cent of the sample so that we have preferred to exclude the SIM + Chabrier combination when discussing the scaling relations. This is a reasonable choice under the hypothesis of a universal IMF which does not depend on galaxy parameters. There are different evidences that this might not be the case, although there is still not any consensus whether the IMF might change with galaxy morphology, luminosity/mass and/or stellar population parameters (Davé 2008; van Dokkum 2008; Holden et al. 2010; Napolitano et al. 2010; van Dokkum & Conroy 2010, 2011). Here we decided to check what can be the impact of the IMF choice, by computing the scaling relations for a mixed sample made out of the 25 lenses in the G sample of the SIM + Chabrier model and the remaining 26 lenses of the G sample of the SIM + Salpeter model. In a sense, we are here postulating an IMF varying with the halo virial mass and approximating such a variation with a rough step function.

Let us consider first the DM column density within R_e. For the best-fitting relations, we get

$$\log \mathcal{S}_{\rm DM}(R_e) = -0.003 \log\left(L_V/10^{11}\,{\rm L}_\odot\right) + 3.21,$$

$$\log \mathcal{S}_{\rm DM}(R_e) = -0.02 \log\left(M_\star/10^{11}\,{\rm M}_\odot\right) + 3.22,$$

$$\log \mathcal{S}_{\rm DM}(R_e) = -0.09 \log R_e + 2.33,$$

$$\log \mathcal{S}_{\rm DM}(R_e) = 0.06 \log\left(M_{200}/10^{12}\,{\rm M}_\odot\right) + 3.11.$$

Comparing with the values in Table 1, we see that the best-fitting relations are shallower for (L_V, $M_\star$) and steeper for (R_e, M_{200}). However, if we consider the 68 per cent confidence ranges, the slopes are fully consistent so that the change in the slope cannot be considered statistically significant.

Similarly, the total column density $\mathcal{S}_{\rm tot}$ turned out to have the best-fitting relations with slopes (−0.21, 0.05, −0.04, −0.04) for (L_V, $M_\star$, R_e, M_{200}), respectively. Also, for these relations the confidence ranges significantly overlap with respect to the Salpeter IMF (see Table 1) thus the two cases do not differ significantly.

For the DM Newtonian acceleration we obtain

$$\log g_{\rm DM}(R_e) = -0.05 \log\left(L_V/10^{11}\,{\rm L}_\odot\right) - 9.45,$$

$$\log g_{\rm DM}(R_e) = -0.07 \log\left(M_\star/10^{11}\,{\rm M}_\odot\right) - 9.42,$$

$$\log g_{\rm DM}(R_e) = -0.13 \log R_e - 9.33,$$

$$\log g_{\rm DM}(R_e) = 0.13 \log\left(M_{200}/10^{12}\,{\rm M}_\odot\right) - 9.67,$$

which are comparable with the results for slope and zero-point as in Table 1. This suggests that the universality (or lack of it) of the DM Newtonian acceleration is not significantly affected by the choice of the IMF (a similar result has been found for the stellar Newtonian acceleration which we do not report here for brevity).

Finally, we have considered the DM mass fraction within R_e and found that

$$\log f_{\rm DM}(R_e) = 0.18 \log\left(L_V/10^{11}\,{\rm L}_\odot\right) - 0.30,$$

$$\log f_{\rm DM}(R_e) = -0.10 \log\left(M_\star/10^{11}\,{\rm M}_\odot\right) - 0.24,$$

$$\log f_{\rm DM}(R_e) = 0.44 \log R_e - 0.70.$$

As expected, these results turned out to be significantly different from the Salpeter IMF case. In particular, the $f_{\rm DM}$–L_V and $f_{\rm DM}$–R_e relations turned out to be shallower, while $f_{\rm DM}$–$M_\star$ has a negative

slope and a significant anticorrelation. This is the consequence of the step of IMF function assumption which produced a significant increase in the $f_{\rm DM}(R_{\rm e})$ for the lower mass systems with the Chabrier with respect to the smaller $f_{\rm DM}(R_{\rm e})$ obtained with the Salpeter IMF assumed for the more massive ones. The same argument applies to the $f_{\rm DM}$–L_V and $f_{\rm DM}$–R_e relations which turned out to be shallower.

As a final remark, we can conclude that scaling relations are overall mildly affected by the IMF assumption in the dynamical/lensing analysis, with correlations being comparable among results obtained either assuming a universal (Salpeter) IMF, or a non-universal mass-dependent IMF (Chabrier for less massive systems and Salpeter for more massive ones). A universal Chabrier IMF seems to be ruled out because it produces too many systems with unrealistically large virial masses for galaxy systems.

5 CONCLUSIONS

While there is a general consensus on the ubiquitous presence of DM in galaxies, there is still an open debate about its mass density distribution and the role it has exactly played in the galaxy formation scenario. These are crucial issues since the exact density distribution and the assembly processes that dark haloes have undergone might tell more on the actual nature of the DM itself. Scaling relations among DM-related quantities and stellar properties may give important hints about the relative interplay between the two main constituents of galaxies.

In this context, what seems particularly intriguing is the existence of some universal properties of the DM quantities like the column density, or even the presence of a characteristic acceleration scale (e.g. Donato et al. 2009; Gentile et al. 2009), which might be related to common formation processes on many mass scales or morphological categories. Recent works have argued either in favour or against the presence of such universal values (B09, CT10, NRT10). Dealing with DM properties, though, means necessarily to deal with indirect, model-dependent quantities, which can make the conclusions on these parameters strongly affected by the particular model adopted. One approach might be to use models that consider the widest range of DM properties derived from the *N*-body cosmological simulations, e.g. from the cuspy profiles predicted by the classical NFW to the 'cored' profiles of the B95 (see e.g. CT10). The disadvantage of this approach is that it gives a partial view of how the DM scaling relations vary in the two extreme regimes without allowing a generalization of the results in case the actual DM properties are in the between.

In an attempt to test more general, theoretically motivated DM halo profiles, like the one proposed by the secondary infall model as implemented in DP09, we have modelled the central velocity dispersion and the projected mass within the Einstein radius of a large sample of ETG lenses at an intermediate redshift ($\langle z\rangle \sim 0.2$).

In particular, the DP09 models adopted a modified secondary infall scenario including (in a semi-analytic way) the effect of angular momentum, dynamical friction and adiabatic collapse of baryons. As a first important result, we have shown that this model is fully compatible with observations of ETG and well performing in the data fitting. This is a significant step forward with respect to previous analyses where SLACS sample have been modelled with standard NFW (CT10), as the main property of the SIM model is to be fully assigned by a single parameter (the virial mass) instead of the two parameters required by more 'standard' halo density models such as NFW (which is specified once the concentration and virial mass are given) or Burkert profile (characterized by the core radius and the central density).

Even if we consider the correlations between the halo parameters for the NFW (Navarro, Frenk & White 1996; Bullock et al. 2001; Hennawi et al. 2007) and Burkert profiles (e.g. Salucci & Burkert 2000), which allow us to rewrite these models as a function of only one parameter (e.g. the virial mass), we have seen that the best fit to the observed quantities turned out to be generally poorer than the one provided by the SIM model (see Section 3), with only NFW providing a somehow similar significance than the SIM model. This is mainly because in the typical mass range spanned by the ETG sample considered here, the SIM model predicts cuspier profiles according to equation (5), i.e. NFW-like or even cuspier.

With this novel DM set-up, we have estimated the DM column density $\mathcal{S}_{\rm DM}(R_{\rm e})$, the Newtonian acceleration $g_{\rm DM}(R_{\rm e})$ and finally the DM mass fraction $f_{\rm DM}(R_{\rm e})$ along with their correlations with the stellar total luminosity, mass and size. The best-fitting relations show that $\mathcal{S}_{\rm DM}(R_{\rm e})$ is almost constant (possibly increasing with, if any) over the range of stellar parameters (L_V, $M_\star$, $R_{\rm e}$) probed by the adopted data set, while it is clearly strongly correlated with the halo mass M_{200}. This result is actually consistent with both G09, claiming to have found a characteristic density scale over a large range of galaxy luminosities, and with B09 who instead have found a correlation with the dark halo mass.

Similarly we have found an even more remarkably constant DM Newtonian acceleration $g_{\rm DM}(R_{\rm e})$ with (L_V, $M_\star$, $R_{\rm e}$), and still a strong correlation of this quantity with the virial mass. In this case, though, the absolute constancy of the $g_{\rm DM}(R_{\rm e})$ does not allow us to justify the correlation with the virial mass but probably says more of some intrinsic properties of the dark matter haloes, and of the non-existence of a universal acceleration scale. In fact, here we have confirmed an evidence formerly revealed in NRT10, that $g_{\rm DM}(R_{\rm e})$ of the ETGs is on average larger than the one obtained for late-type galaxies (e.g. in Donato et al. 2009, having considered that their column densities obtained at the core radius are an upper limit for the same quantity if computed at the $R_{\rm e}$).

As such, one could argue over the existence of a Newtonian acceleration growing with the morphological type and (possibly) with the stellar mass (if including all the Hubble sequence) as well as shown by the trend with M_{200}.

We need to conclude this reasoning with a caveat, underlying all analyses based on model-dependent approaches: all DM quantities correlations against (L_V, $M_\star$, $R_{\rm e}$) are critically dependent on the adopted halo model and stellar IMF (in our case a Salpeter IMF). A direct comparison with previous literature results is complicated by systematic effects due to differences in both the halo model (SIM versus NFW or Burkert) and the radius where the DM quantities are evaluated ($R_{\rm e}$ versus $R_{\rm s}$ or $R_{\rm c}$). In particular, the comparison of results obtained with the SIM model with similar works based on the adoption of the more standard NFW and B95 has highlighted an interesting correlation between the cuspiness of the dark halo and the size of the parent galaxies. In the SIM approach, in fact, larger galaxies seem to assemble in dark haloes having steeper cusps, while more compact massive ETGs are accommodated on shallower cusps. This is an interesting hint that might be cross-checked on hydrodynamical simulations and seems to be a crucial test for the hierarchical model as a whole.

Finally we stress that there are still some weaknesses in the analysis proposed, mainly posed by the limited galaxy sample (e.g. the SLACS sample only probes a quite limited range in both stellar luminosity and mass), and the large uncertainties on the derived

quantities. However, we have considered this to be a benchmark test for more general dark halo model laws based on a simple physically motivated galaxy model. This is the first step of a broader plan to improve the testing along different roads. On one hand, a detailed theoretical investigation is needed to find out quantities that depend as less as possible on both the adopted halo profile and stellar IMF. Similarly, one should check whether the choice of R_e as a reference radius where DM quantities are evaluated is the most convenient one to find a compromise between the need to not extrapolate outside regions directly probed by data and the halo model characteristics. On the other hand, stronger constraints on the slope of the investigated correlations could be obtained by narrowing the uncertainties on the DM quantities. The use of a one-parameter model, like the SIM, is expected to help by eliminating the degeneracies among halo parameters which generally plague the analysis adopting the NFW profiles or similar, and contribute to the overall error budget. A further improvement would be obtained by fitting the full velocity dispersion profile rather than only its aperture value, although such a strategy could be applied only to local ETGs. Finally, a larger sample spanning a wider range in (L_V, $M_\star$, R_e, M_{200}) would allow us to further narrow down the confidence ranges for the slopes of the investigated correlations by both improving the statistics and tracking the different trends better.

Should both constancy with stellar luminosity, mass and size, and independence on the fitting procedure details be successfully demonstrated, one could safely conclude that a proposed quantity is indeed universal and use such a result to constrain galaxy formation and evolution scenarios.

ACKNOWLEDGMENTS

VFC and CT are funded by the Italian Space Agency (ASI) and the Swiss National Science Foundation, respectively.

REFERENCES

Auger M. W., Treu T., Bolton A. S., Gavazzi R., Koopmans L. V. E., Marshall P. J., Bundy K., Moustakas L. A., 2009, ApJ, 705, 1099 (A+09)
Auger M. W., Treu T., Bolton A. S., Gavazzi R., Koopmans L. V. E., Marshall P. J., Moustakas L. A., Burles S., 2010, ApJ, 724, 511
Avila Reese V., Firmani C., Hernandez X., 1998, ApJ, 505, 37
Baarden J. M., Bond J. M., Kaiser N., Szalay A. S., 1986, ApJ, 304, 15
Blumenthal G. R., Faber S. M., Flores R., Primack J. R., 1986, ApJ, 301, 27
Bolton A. S., 2007, ApJ, 665, 105
Boyarsky A., Ruchayskiy O., Iakubovskyi D., Macciò A. V., Malyshev D., 2009, preprint (arXiv:0911.1774) (B09)
Boylan-Kolchin M., Ma C.-P., 2004, MNRAS, 349, 1117
Bullock J. S., Kolatt T. S., Sigad Y., Somerville R. S., Kravtsov A. V., Klypin A. A., Primack J. R., Dekel A., 2001, MNRAS, 321, 559
Burkert A., 1995, ApJ, 447, L25
Busarello G., Capaccioli M., Capozziello S., Longo G., Puddu E., 1997, A&A, 320, 415
Cappellari M. et al., 2006, MNRAS, 366, 1126
Cardone V. F., 2004, A&A, 415, 839
Cardone V. F., Tortora C., 2010, MNRAS, 409, 1570
Cardone V. F., Tortora C., Molinaro R., Salzano V., 2009, A&A, 504, 769
Carroll S. M., Press W. H., Turner E. L., 1992, ARA&A, 30, 499
Cattaneo A., Dekel A., Faber S. M., Guiderdoni B., 2008, MNRAS, 389, 567
Chabrier G., 2001, ApJ, 554, 1274
Conroy C., Wechsler R. H., 2009, ApJ, 696, 620
D'Agostini G., 2005, preprint (arXiv: physics/0511182)
D'Onofrio M., Valentinuzzi T., Secco L., Caimmi R., Bindoni D., 2006, New Astron. Rev., 50, 447
Davé R., 2008, MNRAS, 385, 147
de Vaucouleurs G., 1948, Ann. Astrophys., 11, 247
Dekel A., Birnboim Y., 2006, MNRAS, 368, 2
Del Popolo A., 2009, ApJ, 698, 2093 (DP09)
Del Popolo A., 2010, MNRAS, 408, 1808
Del Popolo A., Kroupa P., 2009, A&A, 502, 733
Donato F. et al., 2009, MNRAS, 397, 1169 (D09)
Eliasdottir A., Møller O., 2007, J. Cosmol. Astropart. Phys., 07, 006
Fukushige T., Makino J., 2001, ApJ, 557, 533
Fukushige T., Kawai A., Makino J., 2004, ApJ, 606, 625
Gentile G., Famaey B., Zhao H. S., Salucci P., 2009, Nat, 461, 627 (G09)
Ghigna S., Moore B., Governato F., Lake G., Quinn T., Stadel J., 2000, ApJ, 544, 616
Gnedin O. Y., Kravtsov A. V., Klypin A. A., Nagai D., 2004, ApJ, 616, 16
Gott J. R., 1975, ApJ, 201, 296
Gunn J. E., 1977, ApJ, 218, 592
Gunn J. R., Gott J. R., 1972, ApJ, 176, 1
Hennawi J. F., Dalal N., Bode P., Ostriker J. P., 2007, ApJ, 654, 714
Hogg D. W., Bovy J., Lang D., 2010, preprint (arXiv:1008.4686)
Holden B. P., van der Wel A., Kelson D. D., Franx M., Illingworth G. D., 2010, ApJ, 724, 714
Hyde J. B., Bernardi M., 2009, MNRAS, 396, 1171
Jing Y. P., Suto Y., 2000, ApJ, 529, L69
Kandrup H. E., 1980, Phys. Rep. 63, 1
Klypin A., Kravtsov A. V., Bullock, James S., Primack J. R., 2001, ApJ, 554, 903
Klypin A., Zhao H. S., Somerville R. S., 2002, ApJ, 573, 597
Komatsu E. et al., 2009, ApJS, 180, 330
Lampeitl H. et al., 2010, MNRAS, 401, 2331
Liddle A., 2004, MNRAS, 351, L49
Mamon G. A., Lokas E. L., 2005, MNRAS, 362, 95
Marinoni C., Hudson M. J., 2002, ApJ, 569, 101
Moore B., Governato F., Quinn T., Stadel J., Lake G., 1998, ApJ, 499, L5
Muñoz-Cuartas J. C., Macciò A., Gottlöber S., Dutton A., 2011, preprint (arXiv:1102.2186)
Napolitano N. R., Capaccioli M., Romanowsky A. J., Douglas N. G., Merrifield M. R., Kujiken K., Arnaboldi M., Freeman K. C., 2005, MNRAS, 357, 691
Napolitano N. R. et al., 2009, MNRAS, 393, 329
Napolitano N. R., Romanowsky A. J., Tortora C., 2010, MNRAS, 405, 2351
Napolitano N. R. et al., 2011, MNRAS, 411, 2035
Navarro J. F., Frenk C. S., White S. D. M., 1996, ApJ, 462, 563
Navarro J. F., Frenk C. S., White S. D. M., 1997, ApJ, 490, 493
Navarro J. F., Hayashi E., Power C., Jenkins A. R., Frenk C. S., White S. D. M., Springel V., Stadel J., Quinn T. R., 2004, MNRAS, 349, 1039
Padmanabhan N. et al., 2004, New Astron., 9, 329
Percival W. J. et al., 2010, MNRAS, 401, 2148
Power C., Navarro J. F., Jenkins A., Frenk C. S., White S. D. M., Springel V., Stadel J., Quinn T., 2003, MNRAS, 338, 14
Prugniel Ph., Simien F., 1997, A&A, 321, 111
Renzini A., Ciotti L., 1993, ApJ, 416, L49
Ryden B., 1988, ApJ, 329, 589
Ryden B. S., Gunn J. E., 1987, ApJ, 318, 15
Salpeter E. E., 1955, ApJ, 121, 161
Salucci P., Burkert A., 2000, ApJ, 537, L9
Sérsic J. L., 1968, Atlas de Galaxies Australes, Obser. Astron. Cordoba
Thomas J., Saglia R. P., Bender R., Thomas D., Gebhardt K., Magorrian J., Corsini E. M., Wegner G., 2009, ApJ, 691, 770
Tortora C., Napolitano N. R., Romanowsky A. J., Capaccioli M., Covone G., 2009, MNRAS, 396, 1132 (T+09)
Tortora C., Napolitano N. R., Romanowsky A. J., Jetzer P., 2010, ApJ, 721, 1

Treu T., Gavazzi R., Gorecki A., Marhsall P. J., Koopmans L. V. E., Bolton A. S., Moustakas L. A., Burles S., 2009, ApJ, 690, 670
Treu T., Auger M. W., Koopmans L. V. E., Gavazzi R., Marshall P. J., Bolton A. S., 2010, ApJ, 709, 119
van Dokkum P. G., 2008, ApJ, 674, 29
van Dokkum P. G., Conroy C., 2010, Nat, 468, 940
van Dokkum P. G., Conroy C., 2011, ApJ, 735, L13

This paper has been typeset from a TEX/LATEX file prepared by the author.